Direct measurement of electron heating in electron-only reconnection in a laboratory mini-magnetosphere

Lucas Rovige [1,*] Filipe D. Cruz [2] Timothy Van Hoomissen [1] Robert S. Dorst [1,3] Carmen G. Constantin [1] Stephen Vincena [1] Luis O. Silva [2] Christoph Niemann [1] and Derek B. Schaeffer [1]

[1]*Department of Physics and Astronomy, University of California, Los Angeles, Los Angeles, California 90095, USA*

[2]*GoLP/Instituto de Plasmas e Fusão Nuclear, Instituto Superior Técnico, Universidade de Lisboa, 1049-001 Lisboa, Portugal*

[3]*Lawrence Livermore National Laboratory, 7000 East Avenue, Livermore, California 94550, USA*

(Received 13 August 2025; accepted 8 April 2026; published 8 May 2026)

We report on the experimental observation of electron heating in electron-only magnetic reconnection in laser-driven laboratory mini-magnetosphere on the Large Plasma Device (LAPD) at the University of California, Los Angeles. In this experiment, a fast-flowing plasma impacts a pulsed magnetic dipole embedded within LAPD's magnetized ambient plasma, creating an ion-scale magnetosphere and driving electron-only magnetic reconnection between the background and dipole field lines. The electron velocity distribution is measured across the reconnection region using noncollective Thomson scattering, enabling determination of electron temperature and density. Significant electron heating is observed in the electron diffusion region, increasing from an initial temperature of 1.8 to 9.5 eV, corresponding to a 40% local conversion of Poynting flux into electron enthalpy flux. Particle-in-cell simulations that provide insights into the heating mechanisms are also presented.

DOI: 10.1103/8ctf-q5n3

Magnetic reconnection [1] is a fundamental plasma process where the breaking and topological rearrangement of magnetic field lines abruptly releases stored magnetic energy to the plasma and drives explosive events in many different environments across the universe, from planetary magnetospheres, pulsars, and solar flares to disruptions in fusion devices and other laboratory experiments. Magnetic reconnection can energize the ions and electrons of the plasma through both directed kinetic energy and thermal heating, and understanding the partition of this energy transfer as well as the mechanisms behind it is necessary to understand the role of reconnection in particle acceleration, heating, and large-scale energy transport in space and astrophysical systems.

Recently, enabled by the high-resolution measurements of the Magnetospheric Multiscale (MMS) Mission [2,3], a regime of magnetic reconnection has been identified in which only electrons participate in the reconnection process while the ion population remains largely decoupled from the dynamics [4,5]. This electron-only reconnection has been observed in regions of Earth's magnetosphere [4,6] and in laboratory experiments [7–10], and has also attracted interest as its dynamics may be relevant as the onset of classical ion-coupled reconnection [11,12] and could also contribute to magnetic-energy transfer at subion scales within turbulent cascades [4,13,14]. In recent work, Lunar magnetic reconnection from mini-magnetospheres formed by the interaction of the solar wind with ion-scale crustal magnetic anomalies has been observed [15], while the demagnetization of the ions and the small, ion-scale size of the system suggested this reconnection was electron-only. This *in situ* observation has been confirmed by subsequent numerical [16] and experimental [10] results reproducing mini-magnetospheres and observing electron-only reconnection. Additionally, the MAVEN mission enabled the detection of many reconnection events in martian mini-magnetospheres [17–20], a majority of which were ion-coupled, but principally because the instruments on MAVEN cannot resolve the electron scale. Nevertheless, it is expected that a significant part of the reconnection events on Mars are electron-only [17,21]; therefore, laboratory experiments of reconnection in mini-magnetospheres would provide valuable insight into electron-only reconnection in a context relevant to the Moon, Mars, and other small-scale magnetospheres such as near Mercury or Ganymede [22,23].

The question of energy conversion in magnetic reconnection is central to understanding its global impact. In symmetric, ion-coupled reconnection [24–27], most dissipation goes into ions, with electrons heated locally near the X line and ions more broadly in the outflows. Guide fields and asymmetries both tend to enhance electron energization [28–31]. In contrast, sub-ion-scale and electron-only systems produce predominantly electron heating [32]: The electron-to-ion heating ratio increases as the system size decreases [33], and Shi *et al.*[7] found that electron-only reconnection converts $\simeq$70% of the inflowing Poynting flux into electron enthalpy, compared with $\simeq$14% in ion-coupled reconnection [26]. Shi *et al.* [8] found that electron heating was dominated by $E_{\parallel}$, consistent with the trend that $E_{\parallel}$ becomes more important as the guide field increases while $E_{\perp}$

*Contact author: lucas.rovige@ensta.fr

dominates in antiparallel configurations [34–36]. Our work further investigates energy conversion in the relatively unexplored regime of electron-only reconnection, in a flow-driven, asymmetric regime without guide field.

In this article, we report the first direct measurement of electron heating during electron-only magnetic reconnection in a laboratory magnetosphere, using noncollective Thomson scattering to obtain spatially and temporally resolved profiles of electron temperature and velocity distribution. This work provides insights into how reconnection fundamentally transforms magnetic energy into particle energy in an asymmetric, antiparallel (no guide-field) configuration, probing key physics of energy conversion in collisionless plasmas. Beyond its fundamental importance, this dynamic is directly relevant to space environments such as the Moon and Mars, where reconnection at ion-scale magnetic anomalies likely occurs on the electron scale. Because *in situ* spacecraft measurements remain sparse and challenging in these regions, our laboratory approach provides critical access to understanding how such systems evolve. We notably observe a fourfold temperature increase in the diffusion region, as well as a significant conversion from the inflowing Poynting flux to the electron enthalpy flux that is estimated to be 40%. Particle-in-cell (PIC) simulations provide more insight into the mechanism leading to electron heating and show that both the energization from the out-of-plane reconnection electric field and a Fermi-like reflection energization from outflowing reconnected field lines contribute to electron heating.

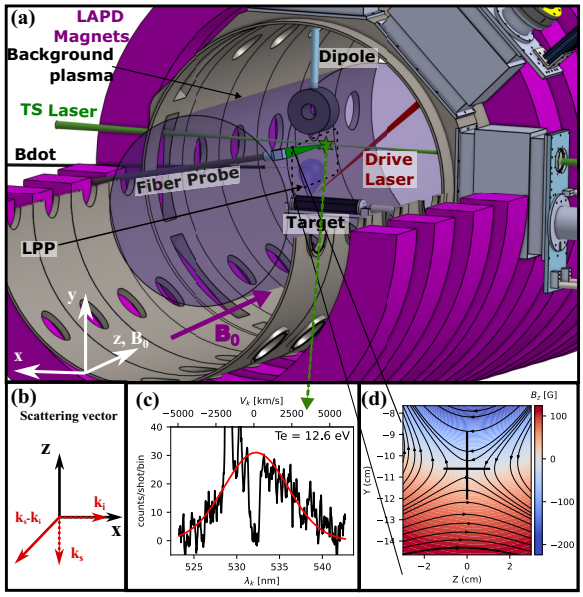

FIG. 1. (a) Schematic of the experiment on the LAPD. (b) Scattering vector $\mathbf{k_s} - \mathbf{k_i}$. (c) Example of a Thomson scattering spectrum obtained by averaging over 400 shots (black) and its Gaussian fit used to retrieve density and temperature (red). (d) Initial magnetic field in the z-direction B_z and magnetic field lines in the reconnection (Y-Z) plane, measured with a B-dot probe. The centered vertical and horizontal lines represent the TS measurement regions.

I. EXPERIMENTAL SETUP AND THOMSON SCATTERING MEASUREMENTS

The experiment is schematized in Fig. 1(a). A high-repetition-rate (1 Hz), 20 ns laser with 10 J of energy per pulse is focused on a graphite target and drives a fast-moving carbon plasma [37,38] that expands into the field generated by a pulsed magnetic dipole embedded into the hydrogen background discharge plasma of density $n_0 = 1.0 \times 10^{13}$ cm^{-3} and axial magnetic field ($\mathbf{B_0} = B_0\hat{\mathbf{z}}$, with $B_0 = 210$ G) generated by the Large Plasma Device (LAPD) [39]. The laser-produced plasma (LPP) expands at a velocity $V_0 = 250$ km/s, corresponding to a super-Alfvenic flow with $M_A = 1.7$. The Larmor radius of the coupled background ions is $\rho_{H^+} = 12.4$ cm $= 1.7d_i$. The field of the dipole oriented to be antiparallel to the background field on the outside, so that a magnetic null point is formed in the region between the dipole and the target at $y = -10.5$ cm ($1.5d_i$), similar to our previous experiment [10]. The time-resolved magnetic field is measured with a magnetic flux (B-dot) probe [40] that is moved between shots to map out the field geometry. We vacuum-mapped the dipole field in the y-z plane and added the uniform LAPD field to plot the baseline magnetic field in the reconnection plane in Fig. 1(d). More comprehensive measurements of the fields and currents are reported in our previous work [10].

In our system, the global dynamics of the system involves motion of the ions. The background ions, along with electrons, are set in forward motion along the y direction by coupling with the laser-produced plasma. Still, the dynamics occurs on subion scales: The typical dipole-field extent is $\sim 1.5d_i = 0.8\rho_i$, and reconnection persists for only a small fraction of the ion gyroperiod ($T_{ci} = 3.1$ μs), while the observed current sheet is electron scale (width $2\delta = 6d_e = 0.1d_i$). Under these conditions, reconnection is expected to occur in the electron-only regime [5], although a weak coupling of the ions through electrostatic Hall fields may still occur [41].

During the experiment, the variation of the magnetic field was measured using a magnetic flux probe that was moved to different position on different laser shots to map out the fields. The magnetic fields were measured in the XY plane and in time, but not in the Z direction because of experimental constraints associated with the Thomson diagnostics. More extensive, volumetric magnetic and electric field data are presented in our previous work [10]. Figure 2 shows the evolution of ΔB_z along the vertical axis and in time, for both the dipole OFF and ON cases. It shows that the magnetic compression at the leading edge of the LPP propagates at 250 km/s in both cases. It shows that the laser-produced plasma flow drives a compression of the magnetic field at its front, while expelling it from the area it is sweeping (diamagnetic cavity). This general dynamics is well understood and has been explored through many previous experiments on the LAPD [37,38,42].

The electron velocity distribution is measured using a scanning noncollective Thomson-scattering (TS) diagnostic [43,44] probing a 2×2 cm^2 region around the reconnection point, using a 0.5 J, 4 ns, 532 nm laser beam propagating along x and a fiber bundle collecting the scattered light, defining a scattering volume $\sim 15 \times 0.1 \times 0.1$ mm^3, so the measurements are well resolved in (y, z) but averaged along x.

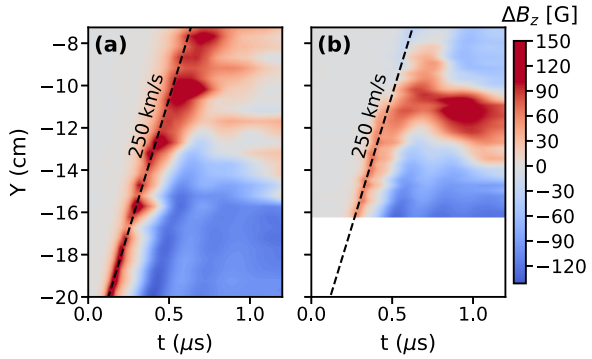

FIG. 2. Variation of z component of the magnetic field ΔB_z along the symmetry axis $xz = 0$ and $z = 0$ and in time, for (a) the "Dipole OFF" case and (b) the "Dipole ON" case. The dashed line highlights a propagation velocity of 250 km/s.

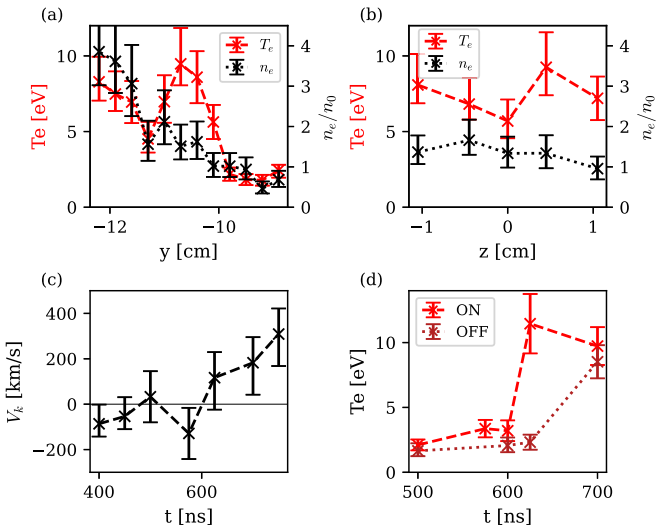

FIG. 3. (a), (b) Electron temperature and density measured by Thomson scattering along the y and z lineouts across the reconnection zone as represented in Fig. 1(c) at $t = 650$ ns. Each position data point is obtained from a spectrum averaged over 400 shots. (c) Electron velocity along $\mathbf{k}$, V_k at $y = -10.5$ cm and $z = -1.5$ cm (outflow) for different times, measured from the Doppler shift of the TS spectra. (d) Electron temperature at the reconnection point $y = -10.5$ cm and $z = 0$ with the dipole turned ON and OFF, for different times of the experiment.

Figure 1(c) shows an example of a TS spectrum and associated velocity distribution, obtained in the LPP. The drop in signal level at the center of the distribution is caused by a physical notch of 1.5 nm width in the spectrometer blocking stray light from the laser at 532 nm. Two emission lines from neutral carbon at 529 and 530 nm are visible in some spectra and removed from the fitting procedure. The electron temperature is estimated by calculating the width of a Gaussian fit of the electron velocity distribution, and the relative density is retrieved from the area under the fitted curve and cross-calibrated with the background density measurement from the interferometer and Langmuir probe. The electron flow-velocity in the scattering direction V_k is obtained by measuring the Doppler shift of the peak of the distribution. The background electron temperature is measured to be $T_{e0} = 1.8 \pm 0.4$ eV. Since the incident vector $\mathbf{k_i}$ is purely along x and the scattering vector $\mathbf{k_s}$ purely along z, the TS measurement vector $\mathbf{k} = \mathbf{k_s} - \mathbf{k_i}$ is at 45° from both x and z axes [see Fig. 1(b)].

Figures 3(a) and 3(b) show the electron temperature and density retrieved from Thomson scattering spectra along the y and z axes, respectively, across the reconnection point located at $y = -10.5$ cm, $z = 0$, at $t = 650$ ns, a time at which magnetic field lines are actively reconnecting. The vertical profile reveals localized electron heating centered around the reconnection point, with a peak temperature of $T_e = 9.5 \pm (^{2.4}_{1.4})$ eV and a corresponding density compression reaching $n_e = 1.5$–$2n_0$. A second region exhibiting similar heating and a stronger, fourfold density enhancement is observed further from the dipole, for $y < -11.3$ cm, associated with the front of the laser-driven plasma. Along the z direction, both temperature and density remain relatively uniform across the current sheet.At the reconnection point, the temperature increase is $\Delta T_e = 7.7 \pm (^{2.4}_{1.4})$ eV compared to a location 1 cm (2δ) away in the y direction. This corresponds to an order of magnitude of the enthalpy production rate $\Delta H = \gamma/(\gamma - 1)\, n_e k_b \Delta T_e\, (2\delta \times 2L)/\tau > 676$ kW/m, with the specific heat ratio $\gamma = 5/3$ (we adopt the standard scalar adiabatic closure, since the measured electron velocity distribution functions remain close to Maxwellian, and remain consistent with Refs. [4,7]), the current sheet width $2\delta = 10$ mm, the current sheet length $2L = 30$ mm, and the electron transit time through the current sheet $\tau = \delta/V_{in} < 28$ ns, where the inflow velocity is assumed to be equal to or larger than the driving flow velocity V_0, providing a lower bound on the enthalpy flux. This can be compared to the dissipated Ohmic power from the reconnection current flow, calculated using the Spitzer resistivity: $P_{\text{Ohm}} = \eta J_x^2\, (2L \times 2\delta) = 7$ kW/m $\sim 0.01 \Delta H$, indicating that the vast majority of the heating is not due to collisional dissipation, but instead arises from collisionless processes. In order to estimate the fraction of magnetic energy going toward heating the electrons, we calculate the ratio of electron enthalpy production to the incoming Poynting flux: $\frac{\gamma/(\gamma-1) n_e k_b \Delta T_e}{B_{\text{rec},z}^2/\mu_0} = 40 \pm (^{13}_{7})\%$, using the peak reconnecting magnetic field measured in Fig. 4(g) on the LPP side: $B_{\text{rec},z} = 0.57 B_0 = 120$ G.

Figure 3(c) displays the electron bulk flow velocity projected along the Thomson scattering vector, V_k, measured at $z = -1.5$ cm and $y = -10.5$ cm, placing it in the outflow region. It shows that after 600 ns, a bulk flow along $+\mathbf{k}$ is measured, with $V_k = 310 \pm (^{110}_{140})$ km/s. Since the projection vector is $\mathbf{k} = -\mathbf{z} - \mathbf{x}$, the positive value V_k is most likely associated with a negative electron outflow V_z, since the electron flow in the x direction is expected to be toward the positive x from the negative reconnection current measured, and therefore contributes negatively to V_k. We assume this contribution from the flow along x is negligible since the measurement is performed on the very edge of the current sheet; therefore, the outflow velocity V_z can be estimated to be $V_z = -\sqrt{2} V_k = -440 \pm (^{200}_{150})$ km/s. This outflow velocity is super-Alfvenic with $V_z = 3V_A$, but significantly lower than the electron Alfven speed $V_z = 0.07 V_{Ae}$. At $t = 750$ ns, part of the LPP has likely reached the measurement point, so the

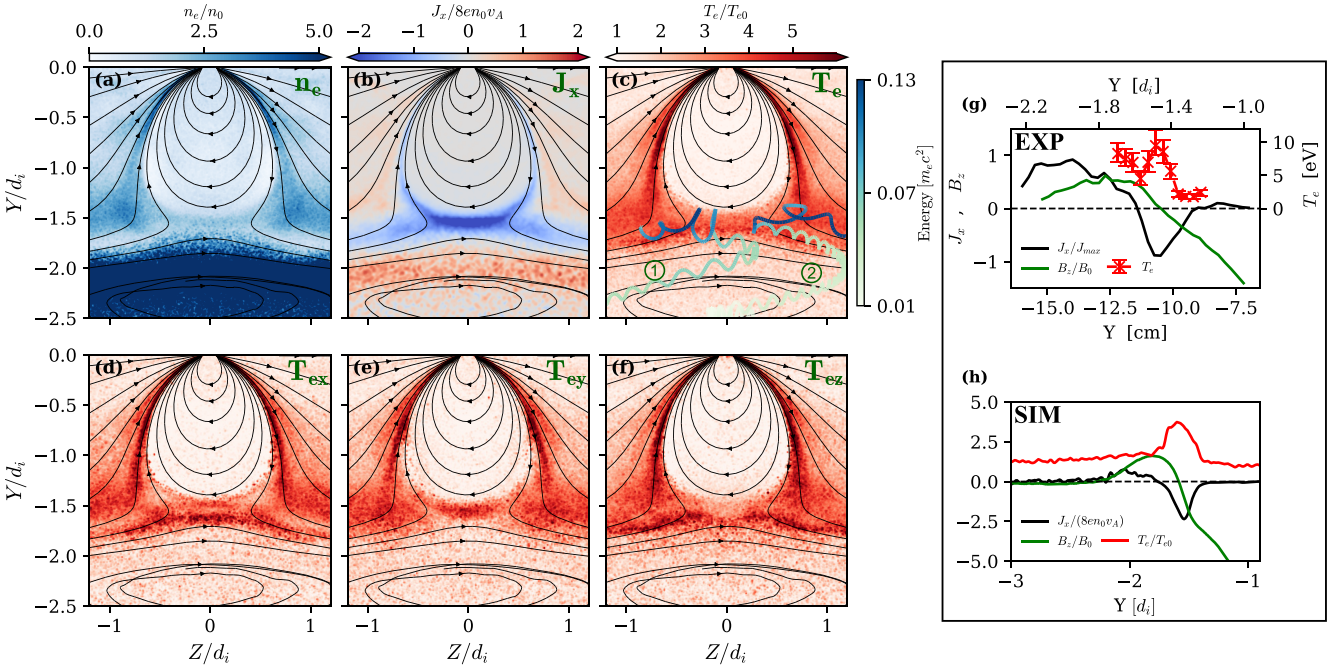

FIG. 4. Simulation result at simulation time $t = 3.9\omega_{ci}^{-1}$ and $x = 0$. The black streamlines represent the magnetic field lines. (a) Normalized electron density. (b) Normalized out-of-plane current density J_x. (c) Electron temperature normalized to the initial temperature. The trajectories of two electrons gaining a significant amount of energy in the reconnection layer are plotted, with their energy in green-blue color scale. (d)–(f) Components of the electron temperature T_{ex}, T_{ey}, T_{ez}, respectively, along the x, y, z directions, normalized to the initial temperature. (g), (h) Vertical lineouts of the out of plane current J_x (black), reconnection magnetic field B_z (green) and electron temperature T_e (red): (top) in the experiment, at $t = 650$ ns, and (bottom) in the simulation.

measured outflow velocity may include a contribution from the predominantly forward (x-directed) LPP motion that we cannot fully disentangle.

Finally, Fig. 3(d) shows that when the dipole, and thus reconnection, is turned off no significant heating is observed at $y = -10.5$ cm, $z = 0$, and $t = 625$ ns while the temperature has increased to $T_e = 11.5 \pm 2$ eV when the dipole is on, confirming this heating is due to magnetic reconnection. Later on, a higher temperature is also measured in the OFF case, associated with the propagation of the hot LPP inside the measurement region.

II. PIC SIMULATIONS AND DISCUSSION

To investigate the mechanisms leading to the heating, we carried out three-dimensional (3D) PIC simulations reproducing the experiment using the code osiris [45], using a reduced mass ratio $m_p/m_e = 100$. In the simulations, a carbon plasma slab modeling the laser-produced plasma moves toward a dipolar field through a region of magnetized ambient hydrogen plasma, at a velocity v_{0d} so that the Alfvénic Mach number is $M_A = 1.5$.

Figure 4 shows two-dimensional (2D) maps of different simulation quantities at a time when reconnection is occurring, and where the piston plasma is close to the reconnection point, as can be seen through the uniform slab of elevated electron density in panel (a). A strong electron scale reconnection current sheet forms at $y = -1.55d_i$ with a width $2\delta \sim 2d_e = d_i/5$ [see Fig. 4(b)]. Figure 4(c) shows significant heating of the electrons to a peak temperature $T_e \sim 3.7T_{e0}$ around the reconnection point, in a zone of width similar to the current sheet, as well as in the outflows and the wings of the magnetosphere. This represents a temperature gain $\Delta T = 3.7T_{e0} - 1.2T_{e0}$ from a distance of 3δ in y (toward the inside of the magnetosphere), yielding a ratio of electron enthalpy production to the incoming Poynting flux (see Supplemental Material [46]): $\frac{\gamma/(\gamma-1)n_e k_b \Delta T_e}{B_{\text{rec},z}^2/\mu_0} = 49\%$, which is comparable to what we measured experimentally. This fraction of the energy contributing to heating the electrons can be compared to previous experimental work. Yamada *et al.* [26] observed 14% of the Poynting flux going to the electron enthalpy in ion-coupled reconnection without guide field. On the other hand, Shi *et al.* [7] observed a conversion of 70% toward electron heating in electron-only reconnection with a strong guide field. Yamada *et al.* carried out a global, ion-scale energy inventory across a multi-d_i control volume including the exhaust, while Shi *et al.* compared local temperature increases with Poynting flux at electron scales. Because our analysis follows this local methodology, it is directly comparable to Shi *et al.*, whereas the magnetic reconnection experiment (MRX) result provides a more qualitative reference from a distinct regime. Figures 4(g) and 4(h) show a comparison of vertical lineouts of reconnection magnetic field, current, and electron temperature in the experiment and in the simulation, highlighting their good agreement, with a localized heating around the magnetic null point and reconnection current sheet.

Comparing the different components of the electron temperature in Figs. 4(d)–4(f) reveals directional anisotropies that provide insight into the mechanisms responsible for the heating. Most of the anisotropy is localized near the recon-

nection point, where the temperature is dominated by T_{ex}. This points toward the reconnection electric field E_x being responsible of energizing electrons as they enter the electron diffusion region (EDR) and become unmagnetized. In the outflow regions, the parallel electron temperature component T_{ez} dominates, reaching approximately $T_{ez} \sim 1.3T_e$. Farther downstream in the exhaust, the electron temperature becomes isotropic again, with all three components contributing comparably. We tracked electrons from the simulation that went through the reconnection region and gained significant energy. The trajectories of two of these electrons are represented over the temperature map in Fig. 4(c). Trajectory ① is typical of an electron accelerated by the reconnection electric field E_x [35,47–49]; as it enters the diffusion region, it gets trapped in the magnetic well and meanders across the width of the current sheet, thus spending more time interacting with E_x. Trajectory ② is typical of another heating mechanism in the outflows, similar to the Fermi-acceleration process [50,51], where electrons travel along field lines toward the reconnection point and reflect at the line's end. As the newly reconnected field line contracts and straightens outward at the outflow velocity, it imparts an additional kick to the electron in the z direction during reflection. The significant contribution of this mechanism to the heating is an important difference from what has been recently observed on PHASMA [8] in electron-only reconnection where the presence of a strong guide field was preventing its efficiency.

III. CONCLUSIONS

These results demonstrate an important electron heating associated with electron-only magnetic reconnection in mini-magnetospheres. We observe a conversion of 40% of the incoming Poynting flux into electron enthalpy in the current sheet (49% in the simulation). While this measurement provides an initial quantitative picture, further work carrying out a more systematic and global energy balance would be beneficial to understand energy transfer in electron-only magnetic reconnection. PIC simulations suggest that electron heating could be sustained by two distinct processes. First, electrons gain energy directly from the reconnection electric field inside the EDR mechanism previously identified as dominant for electron-only reconnection with a strong guide field [7,8]. Second, a Fermi-type acceleration operating in the outflow jets contributes significantly, which was not the case on previous experiments because the presence of a strong guide field suppressed it [8]. Future experiments will assess the experimental relevance and relative importance of these mechanisms in mini-magnetospheres through measurements of electron-temperature anisotropy during antiparallel, electron-only reconnection.

ACKNOWLEDGMENTS

The experiments were performed at the UCLA Basic Plasma Science Facility (BaPSF), which is a collaborative research facility funded by the U.S. Department of Energy, Fusion Energy Sciences program, with additional support by the National Science Foundation. The authors are grateful to the staff of the BaPSF for their help in carrying out these experiments. The experiments were supported by the NSF/DOE Partnership in Basic Plasmas Science and Engineering Awards No. PHY-2320946 and No. PHY-2409284, and DOE Award No. DE-FOA-0002982 (LaserNetUS). This work is supported by the Portuguese Science Foundation (FCT), under the Project No. 2022.02230.PTDC (X-MASER) and the Ph.D. Fellowship Grant No. UI/BD/154620/2022. Simulations were performed at Deucalion (Portugal), funded by FCT Masers in Astrophysical Plasmas (MAPs) i.P. Project No. 2024.11062.cPcA.A3.

DATA AVAILABILITY

The data that support the findings of this article are not publicly available. The data are available from the authors upon reasonable request.

APPENDIX A: ADDITIONAL EXPERIMENTAL DATA

Figure 5 shows that the compression from the LPP pushes the null-point forward starting at $t = 550$ ns and evolves on a timescale on the order of ∼100 ns.

Figure 6 shows the current density J_x in the XY plane at a time $t = 650$ ns where reconnection is occurring. It clearly shows a negative reconnection current sheet at $\sim Y = 10$ cm, from which we can identify the current sheet thickness $2\delta = 10$ mm. The width of the current sheet in not visible in this plot as this shows the plane perpendicular to the reconnection plane (YZ).

APPENDIX B: SIMULATION SETUP

The 3D PIC simulation presented in this work was carried out using the PIC code osiris [45]. The simulations reproduce the interaction of an unmagnetized driver plasma with a background plasma immersed in both a uniform internal magnetic field $\mathbf{B}_0$ and an externally applied dipolar magnetic field $\mathbf{B}_d$ (see Fig. 7). A computational domain spanning $10d_i \times 12d_i \times 18d_i$ was used with grid spacing $\Delta x = 0.1d_e = 0.01d_i$, corresponding to $1000 \times 1200 \times 1800$ cells, and eight parti-

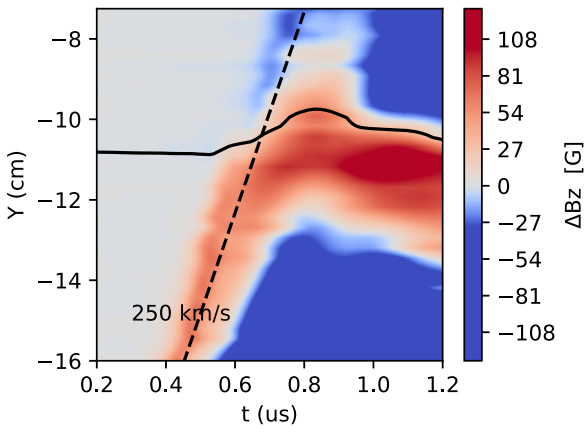

FIG. 5. Enlarged and saturated version of Fig. 2(b) that highlights magnetic field variation around the null point. The solid line represent the evolution of the position of the magnetic null point in time.

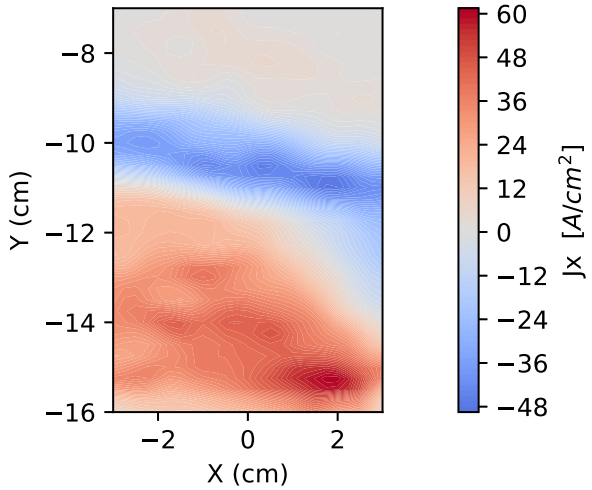

FIG. 6. Partial current density J_x in the XY plane at $t = 650$ ns, obtained from the magnetic field data $J = \frac{1}{\mu_0}\nabla \times \Delta B$, missing the ∂z component as it was calculated from a 2D plane.

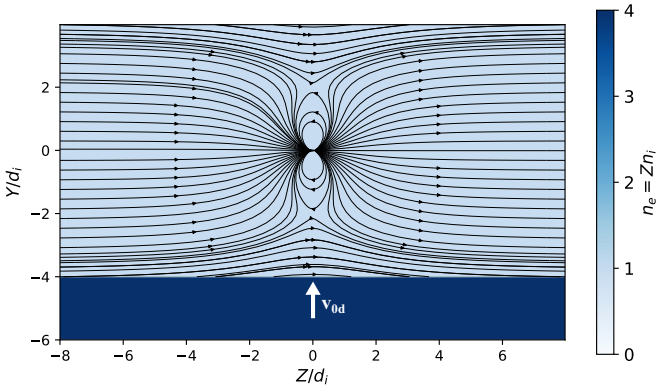

FIG. 7. Slice at $x = 0$ of the initialization of the PIC simulation. The magnetic field lines are shown in black, and the electron density in blue. The driver plasma slab is initialized with a uniform velocity along y: $v_{0d} = 0.043c$.

cles per cell. The simulation time step is $dt = 0.05761/\omega_{pe}$ and particles are interpolated with a cubic function.

The driver plasma moves in the y direction with a flow velocity of $v_{d0} = 0.043c$ and it is located between $-6 < y/d_i < -4$, while the background plasma is located between $-4 < y/d_i < 4$. Both plasmas have an infinite width. To simulate the carbon target, the driver ions have a charge of $+4$ and an ion-to-electron mass ratio of $m_{id}/m_e = 1200$, while the background ions have a charge of $+1$ and mass ratio of $m_{i0}/m_e = 100$. The plasmas have uniform and equal ion density $n_{d0} = n_0$. The ratio $T_e/m_e v_{d0}^2 \sim 5$ and $T_e = T_i$ is comparable to the experiment. In the simulation, the plasma beta is $\beta_{\text{sim}} = 0.2$, which is larger than the experimental beta $\beta_{\text{exp}} = 0.03$, but remains in the low plasma beta regime. Moreover, additional 2D simulations with a lower plasma beta did not show a large change in the dynamics when going from $\beta = 0.2$ to $\beta = 0.03$.

$\mathbf{B_0}$ and $\mathbf{B_d}$ are set to be antiparallel in the z direction. $\mathbf{B_0} = B_0\ \hat{\mathbf{z}}$ was chosen such that the Alfénic Mach number $M_A = v_{0d}\sqrt{\mu_0 n_0 m_{i0}}/B_0$ is equal to 1.5. The dipole is centered at $\{y, z, x\} = \{0, 0, 0\}$ and the dipolar magnetic moment was chosen such that the magnetosphere's standoff distance is $L_M = d_i$, leading to an initial null magnetic field at $y \approx -2.0\ d_i$.

[1] M. Yamada, R. Kulsrud, and H. Ji, Magnetic reconnection, Rev. Mod. Phys. **82**, 603 (2010).

[2] J. L. Burch, R. B. Torbert, T. D. Phan, L.-J. Chen, T. E. Moore, R. E. Ergun, J. P. Eastwood, D. J. Gershman, P. A. Cassak, M. R. Argall, *et al.*, Electron-scale measurements of magnetic reconnection in space, Science **352**, aaf2939 (2016).

[3] F. D. Wilder, R. E. Ergun, S. Eriksson, T. D. Phan, J. L. Burch, N. Ahmadi, K. A. Goodrich, D. L. Newman, K. J. Trattner, R. B. Torbert, B. L. Giles, R. J. Strangeway, W. Magnes, P.-A. Lindqvist, and Y.-V. Khotyaintsev, Multipoint measurements of the electron jet of symmetric magnetic reconnection with a moderate guide field, Phys. Rev. Lett. **118**, 265101 (2017).

[4] T. D. Phan, J. P. Eastwood, M. A. Shay, J. F. Drake, B. U. Ö. Sonnerup, M. Fujimoto, P. A. Cassak, M. Øieroset, J. L. Burch, R. B. Torbert, *et al.*, Electron magnetic reconnection without ion coupling in Earth's turbulent magnetosheath, Nature (London) **557**, 202 (2018).

[5] P. Sharma Pyakurel, M. A. Shay, T. D. Phan, W. H. Matthaeus, J. F. Drake, J. M. TenBarge, C. C. Haggerty, K. G. Klein, P. A. Cassak, T. N. Parashar, M. Swisdak, and A. Chasapis, Transition from ion-coupled to electron-only reconnection: Basic physics and implications for plasma turbulence, Phys. Plasmas **26**, 082307 (2019).

[6] H. Y. Man, M. Zhou, Y. Y. Yi, Z. H. Zhong, A. M. Tian, X. H. Deng, Y. Khotyaintsev, C. T. Russell, and B. L. Giles, Observations of electron-only magnetic reconnection associated with macroscopic magnetic flux ropes, Geophys. Res. Lett. **47**, e2020GL089659 (2020).

[7] P. Shi, P. Srivastav, M. H. Barbhuiya, P. A. Cassak, E. E. Scime, and M. Swisdak, Laboratory observations of electron heating and non-Maxwellian distributions at the kinetic scale during electron-only magnetic reconnection, Phys. Rev. Lett. **128**, 025002 (2022).

[8] P. Shi, E. E. Scime, M. H. Barbhuiya, P. A. Cassak, S. Adhikari, M. Swisdak, and J. E. Stawarz, Using direct laboratory measurements of electron temperature anisotropy to identify the heating mechanism in electron-only guide field magnetic reconnection, Phys. Rev. Lett. **131**, 155101 (2023).

[9] A. Chien, L. Gao, S. Zhang, H. Ji, E. G. Blackman, W. Daughton, A. Stanier, A. Le, F. Guo, R. Follett, *et al.*, Non-thermal electron acceleration from magnetically driven reconnection in a laboratory plasma, Nat. Phys. **19**, 254 (2023).

[10] L. Rovige, F. D. Cruz, R. S. Dorst, J. J. Pilgram, C. G. Constantin, S. Vincena, F. Cruz, L. O. Silva, C. Niemann, and D. B. Schaeffer, Laboratory study of magnetic reconnection in lunar-relevant mini-magnetospheres, Astrophys. J. **969**, 124 (2024).

[11] M. Hubbert, C. T. Russell, Y. Qi, S. Lu, J. L. Burch, B. L. Giles, and T. E. Moore, Electron-only reconnection as a transition phase from quiet magnetotail current sheets to traditional magnetotail reconnection, J. Geophys. Res.: Space Phys. **127**, e2021JA029584 (2022).

[12] S. Lu, Q. Lu, R. Wang, P. L. Pritchett, M. Hubbert, Y. Qi, K. Huang, X. Li, and C. T. Russell, Electron-only reconnection as a transition from quiet current sheet to standard reconnection in Earth's magnetotail: Particle-in-cell simulation and application to MMS data, Geophys. Res. Lett. **49**, e2022GL098547 (2022).

[13] F. Califano, S. S. Cerri, M. Faganello, D. Laveder, M. Sisti, and M. W. Kunz, Electron-only reconnection in plasma turbulence, Front. Phys. **8**, 317 (2020).

[14] Z. Liu, C. Silva, L. M. Milanese, M. Zhou, N. R. Mandell, and N. F. Loureiro, Electron-only magnetic reconnection and inverse magnetic-energy transfer at subion scales, Phys. Rev. Lett. **134**, 155201 (2025).

[15] R. P. Sawyer, J. S. Halekas, J. W. Bonnell, L. J. Chen, J. McFadden, K. H. Glassmeier, Y. Harada, and A. Stanier, Does magnetic reconnection occur in the near lunar surface environment?, Geophys. Res. Lett. **50**, e2023GL104733 (2023).

[16] A. Stanier, L. J. Chen, A. Le, J. Halekas, and R. Sawyer, Intermittent electron-only reconnection at lunar minimagnetospheres, Astrophys. J. Lett. **963**, L11 (2024).

[17] Y. Harada, J. S. Halekas, J. P. McFadden, J. Espley, G. A. DiBraccio, D. L. Mitchell, C. Mazelle, D. A. Brain, L. Andersson, Y. J. Ma, D. E. Larson, S. Xu, T. Hara, S. Ruhunusiri, R. Livi, and B. M. Jakosky, Survey of magnetic reconnection signatures in the Martian magnetotail with MAVEN, J. Geophys. Res.: Space Phys. **122**, 5114 (2017).

[18] Y. Harada, J. S. Halekas, G. A. DiBraccio, S. Xu, J. Espley, J. P. Mcfadden, D. L. Mitchell, C. Mazelle, D. A. Brain, T. Hara, Y. J. Ma, S. Ruhunusiri, and B. M. Jakosky, Magnetic reconnection on dayside crustal magnetic fields at Mars: MAVEN observations, Geophys. Res. Lett. **45**, 4550 (2018).

[19] J. Wang, J. Yu, X. Xu, J. Cui, J. Cao, Y. Ye, Q. Xu, M. Wang, Z. Zhou, Q. Chang, J. Xu, and X. Wang, MAVEN observations of magnetic reconnection at Martian induced magnetopause, Geophys. Res. Lett. **48**, e2021GL095426 (2021).

[20] X. Qiu, Y. Yu, J. Wang, L. Chai, F. Gong, L. Liu, and J. Cao, Observations of the crustal mini-magnetopause reconnection at Mars, Astrophys. J. **977**, 109 (2024).

[21] L. Wang, C. Huang, A. Du, Y. Ge, G. Chen, J. Fan, and J. Qin, Magnetic reconnection in the Martian magnetotail: Occurrence rate and impact on ion loss, Geophys. Res. Lett. **50**, e2023GL104996 (2023).

[22] J. A. Slavin, S. M. Krimigis, M. H. Acuña, B. J. Anderson, D. N. Baker, P. L. Koehn, H. Korth, S. Livi, B. H. Mauk, S. C. Solomon, and T. H. Zurbuchen, MESSENGER: Exploring Mercury's magnetosphere, Space Sci. Rev. **131**, 133 (2007).

[23] R. W. Ebert, S. A. Fuselier, F. Allegrini, F. Bagenal, S. J. Bolton, G. Clark, J. E. P. Connerney, G. A. DiBraccio, W. S. Kurth, S. Levin, D. J. McComas, J. Montgomery, N. Romanelli, A. H. Sulaiman, J. R. Szalay, P. Valek, and R. J. Wilson, Evidence for magnetic reconnection at Ganymede's upstream magnetopause during the PJ34 Juno flyby, Geophys. Res. Lett. **49**, e2022GL099775 (2022).

[24] N. Aunai, G. Belmont, and R. Smets, Energy budgets in collisionless magnetic reconnection: Ion heating and bulk acceleration, Phys. Plasmas **18**, 122901 (2011).

[25] J. P. Eastwood, T. D. Phan, J. F. Drake, M. A. Shay, A. L. Borg, B. Lavraud, and M. G. G. T. Taylor, Energy partition in magnetic reconnection in Earth's magnetotail, Phys. Rev. Lett. **110**, 225001 (2013).

[26] M. Yamada, J. Yoo, J. Jara-Almonte, H. Ji, R. M. Kulsrud, and C. E. Myers, Conversion of magnetic energy in the magnetic reconnection layer of a laboratory plasma, Nat. Commun. **5**, 4774 (2014).

[27] S. Bose, W. Fox, H. Ji, J. Yoo, A. Goodman, A. Alt, and M. Yamada, Conversion of magnetic energy to plasma kinetic energy during guide field magnetic reconnection in the laboratory, Phys. Rev. Lett. **132**, 205102 (2024).

[28] H. Tanabe, T. Yamada, T. Watanabe, K. Gi, K. Kadowaki, M. Inomoto, R. Imazawa, M. Gryaznevich, C. Michael, B. Crowley, N. J. Conway, R. Scannell, J. Harrison, I. Fitzgerald, A. Meakins, N. Hawkes, K. G. McClements, T. O'Gorman, C. Z. Cheng, Y. Ono, and The MAST Team, Electron and ion heating characteristics during magnetic reconnection in the MAST spherical tokamak, Phys. Rev. Lett. **115**, 215004 (2015).

[29] K. J. Genestreti, J. L. Burch, P. A. Cassak, R. B. Torbert, R. E. Ergun, A. Varsani, T. D. Phan, B. L. Giles, C. T. Russell, S. Wang, M. Akhavan-Tafti, and R. C. Allen, The effect of a guide field on local energy conversion during asymmetric magnetic reconnection: MMS observations, J. Geophys. Res.: Space Phys. **122**, 11,342 (2017).

[30] J. Yoo, B. Na, J. Jara-Almonte, M. Yamada, H. Ji, V. Roytershteyn, M. R. Argall, W. Fox, and L.-J. Chen, Electron heating and energy inventory during asymmetric reconnection in a laboratory plasma, J. Geophys. Res.: Space Phys. **122**, 9264 (2017).

[31] M. Yamada, L.-J. Chen, J. Yoo, S. Wang, W. Fox, J. Jara-Almonte, H. Ji, W. Daughton, A. Le, J. Burch, B. Giles, M. Hesse, T. Moore, and R. Torbert, The two-fluid dynamics and energetics of the asymmetric magnetic reconnection in laboratory and space plasmas, Nat. Commun. **9**, 5223 (2018).

[32] N. Wild, W. Gekelman, and R. L. Stenzel, Resistivity and energy flow in a plasma undergoing magnetic-field-line reconnection, Phys. Rev. Lett. **46**, 339 (1981).

[33] S. Roy, R. Bandyopadhyay, W. H. Matthaeus, and P. S. Pyakurel, Energy dissipation in electron-only reconnection, Astrophys. J. **964**, 44 (2024).

[34] N. Bessho, L.-J. Chen, K. Germaschewski, and A. Bhattacharjee, Electron acceleration by parallel and perpendicular electric fields during magnetic reconnection without guide field, J. Geophys. Res.: Space Phys. **120**, 9355 (2015).

[35] A. Le, J. Egedal, and W. Daughton, Two-stage bulk electron heating in the diffusion region of anti-parallel symmetric reconnection, Phys. Plasmas **23**, 102109 (2016).

[36] V. Wilder, R. E. Ergun, J. L. Burch, N. Ahmadi, S. Eriksson, T. D. Phan, K. A. Goodrich, J. Shuster, A. C. Rager, R. B. Torbert, B. L. Giles, R. J. Strangeway, F. Plaschke, W. Magnes, P. A. Lindqvist, and Y. V. Khotyaintsev, The role of the parallel electric field in electron-scale dissipation at reconnecting currents in the magnetosheath, J. Geophys. Res.: Space Phys. **123**, 6533 (2018).

[37] C. Niemann, W. Gekelman, C. G. Constantin, E. T. Everson, D. B. Schaeffer, S. E. Clark, D. Winske, A. B. Zylstra, P.

Pribyl, S. K. P. Tripathi, D. Larson, S. H. Glenzer, and A. S. Bondarenko, Dynamics of exploding plasmas in a large magnetized plasma, Phys. Plasmas **20**, 012108 (2013).

[38] D. B. Schaeffer, A. S. Bondarenko, E. T. Everson, S. E. Clark, C. G. Constantin, and C. Niemann, Characterization of laser-produced carbon plasmas relevant to laboratory astrophysics, J. Appl. Phys. **120**, 043301 (2016).

[39] W. Gekelman, P. Pribyl, Z. Lucky, S. Vincena, B. V. Compernolle, T. A. Carter, and D. Leneman, The upgraded Large Plasma Device, a machine for studying frontier basic plasma physics, Rev. Sci. Instrum. **87**, 025105 (2016).

[40] E. T. Everson, P. Pribyl, C. G. Constantin, A. Zylstra, D. Schaeffer, N. L. Kugland, and C. Niemann, Design, construction, and calibration of a three-axis, high-frequency magnetic probe (*B*-dot probe) as a diagnostic for exploding plasmas, Rev. Sci. Instrum. **80**, 113505 (2009).

[41] Y. Guan, Q. Lu, S. Lu, Y. Shu, and R. Wang, Role of ion dynamics in electron-only magnetic reconnection, Geophys. Res. Lett. **51**, e2024GL110787 (2024).

[42] D. B. Schaeffer, F. D. Cruz, R. S. Dorst, F. Cruz, P. V. Heuer, C. G. Constantin, P. Pribyl, C. Niemann, L. O. Silva, and A. Bhattacharjee, Laser-driven, ion-scale magnetospheres in laboratory plasmas. I. Experimental platform and first results, Phys. Plasmas **29**, 042901 (2022).

[43] S. Ghazaryan, M. Kaloyan, W. Gekelman, Z. Lucky, S. Vincena, S. K. P. Tripathi, P. Pribyl, and C. Niemann, Thomson scattering on the Large Plasma Device, Rev. Sci. Instrum. **93**, 083514 (2022).

[44] H. Zhang, J. J. Pilgram, C. G. Constantin, L. Rovige, P. V. Heuer, S. Ghazaryan, M. Kaloyan, R. S. Dorst, D. B. Schaeffer, and C. Niemann, Two-dimensional Thomson scattering in laser-produced plasmas, Instruments **7**, 25 (2023).

[45] R. A. Fonseca, L. O. Silva, F. S. Tsung, V. K. Decyk, W. Lu, C. Ren, W. B. Mori, S. Deng, S. Lee, T. Katsouleas, and J. C. Adam, OSIRIS: A three-dimensional, fully relativistic particle in cell code for modeling plasma based accelerators, in *Computational Science—ICCS 2002* (Springer, Berlin, Heidelberg, 2002), pp. 342–351.

[46] See Supplemental Material at http://link.aps.org/supplemental/10.1103/8ctf-q5n3 for details on the derivation of the expression.

[47] M. Hesse, K. Schindler, J. Birn, and M. Kuznetsova, The diffusion region in collisionless magnetic reconnection, Phys. Plasmas **6**, 1781 (1999).

[48] P. Ricci, G. Lapenta, and J. U. Brackbill, Electron acceleration and heating in collisionless magnetic reconnection, Phys. Plasmas **10**, 3554 (2003).

[49] J. Egedal, W. Daughton, and A. Le, Large-scale electron acceleration by parallel electric fields during magnetic reconnection, Nat. Phys. **8**, 321 (2012).

[50] J. F. Drake, M. Swisdak, H. Che, and M. A. Shay, Electron acceleration from contracting magnetic islands during reconnection, Nature (London) **443**, 553 (2006).

[51] J. T. Dahlin, J. F. Drake, and M. Swisdak, The mechanisms of electron heating and acceleration during magnetic reconnection, Phys. Plasmas **21**, 092304 (2014).